Eur. Phys. J. D (2014) 68: 168
DOI: 10.1140/epjd/e2014-50277-1

THE EUROPEAN PHYSICAL JOURNAL D

Regular Article

Measurement of the Aharonov-Casher geometric phase with a separated-arm atom interferometer

Jonathan Gillot, Steven Lepoutre, Alexandre Gauguet, Jacques Vigué, and Matthias Büchner[a]

Laboratoire Collisions Agrégats Réactivité-IRSAMC, Université de Toulouse-UPS and CNRS UMR 5589, 31062 Toulouse, France

Received 11 December 2013
Published online 27 June 2014 –

Abstract. In this letter, we report a measurement of the Aharonov-Casher (AC) geometric phase with our lithium atom interferometer. The AC phase appears when a particle carrying a magnetic dipole propagates in a transverse electric field. The first measurement of the AC phase was done with a neutron interferometer in 1989 by Cimmino et al. [Phys. Rev. Lett. **63**, 380 (1989)] and all the following experiments were done with Ramsey or Ramsey-Bordé interferometers with molecules or atoms. In our experiment, we use lithium atoms pumped in a single hyperfine-Zeeman sublevel and we measure the AC-phase by applying opposite electric fields on the two interferometer arms. Our measurements are in good agreement with the expected theoretical values and they also provide a further test of the independence of the AC phase with the atom velocity.

1 Introduction

In 1984, Aharonov and Casher [1] discovered the geometric phase which is called by their name. This phase appears when a particle with a magnetic dipole interacts with an electric field perpendicular to both the particle velocity and to the magnetic dipole. This phase had also been discussed by Anandan [2], who did not remark its unusual properties. The Aharonov-Casher (AC) phase is the second example of a geometric phase, after the Aharonov-Bohm phase [3]. A third geometric phase has been predicted in 1993/1994 by He and McKellar [4] and by Wilkens [5] and is now named the He-McKellar-Wilkens (HMW) phase. We have recently measured this phase [6,7]. This phase appears, if an electric dipole travels in a magnetic field $\mathbf{B}$ and if the mixed product of the dipole, $\mathbf{B}$ and the velocity vectors is not zero. All these phases belong to the general class of geometric phases discussed by Berry in 1984 [8,9] and they are very interesting because they strongly differ from dynamical phases: geometric phases modify the wave propagation in the absence of any force on the particle; they are independent of the modulus of the particle velocity but they change sign if the velocity is reversed.

In the present letter, we describe measurements of the AC phase shift with a separated-arm ^{7}Li atom interferometer using Bragg diffraction on laser standing waves. The internal quantum state of the atom is the same in the two interferometer arms and we apply opposite electric fields and a common magnetic field on the two interferometer arms. The atom fringes are phase shifted by both the AC and the HMW phases. The AC phase is proportional to the atom magnetic dipole moment, thus depends on the magnetic sublevel, while the HMW phase is independent of the sublevel. By combining measurements made with the ^{7}Li atoms pumped in the sublevels of the $F = 2$ level, either in $m_F = +2$ or in $m_F = -2$, we can extract both phases. In the present paper, we focus on the AC phase measurements. As explained below, our experiment is the first phase measurement performed with atoms which is able to test the topological nature of this phase. The sensitivity of our atom interferometer has enabled us to verify the velocity dependence of this phase.

2 Previous measurements of the Aharonov-Casher

Since its theoretical discovery, the AC phase has been tested in five different experiments [10–15]. We recall in Table 1 the main parameters of these experiments.

The first experiment done in 1989 by Cimmino et al. [10] was performed with a neutron interferometer operating with unpolarized neutrons and supplementary phase shifts of magnetic and gravitational origins were needed in order to measure a spin-dependent phase with unpolarized neutrons. The measurement of such a small phase shift with a neutron interferometer was a real tour de force which allowed to demonstrate for the first time the AC phase within 24% of accuracy.

The four following experiments were based on Ramsey or Ramsey-Bordé interferometry with atoms or molecules. In these experiments, the atom or molecule propagates in a quantum superposition of internal states with different

[a] e-mail: matthias.buchner@irsamc.ups-tlse.fr

Table 1. Measurements of the AC phase. μ is the magnetic dipole moment and μ_B the Bohr magneton. E_{max} is the maximum electric field strength, $\varphi_{AC,max}$ is the maximum AC phase and v is the particle velocity. References [14,15] did not probe the same quantum superposition configuration, which explains the larger ratio $\varphi_{AC,max}/E_{max}$ of [15].

Species	μ/μ_B	E_{max} (MV/m)	$\varphi_{AC,max}$ (mrad)	error (%)	v (m/s)
n [10]	1.0×10^{-3}	30	2.19	24	2680
TlF [11]	1.4×10^{-3}	3	2.22	4	220–340
TlF [12]	1.4×10^{-3}	2	2.42	2	188–366
^{85}Rb [13]	1/3	0.9	150	1.4	300–650
^{40}Ca [14]	3/2	1	35	2.2	643–698
^{40}Ca [15]	3/2	4.4	314	2.9	650, 810
^{7}Li (this work)	1	0.9	68	2.1	744–1520

magnetic moments and the AC phase shift appears directly as a shift of the fringe signal.

We do not use such quantum superpositions in our experiment: the atom is in the same internal quantum state in the two interferometer arms.

3 Theoretical value of the Aharonov-Casher phase

The AC phase is given by [1]:

$$\varphi_{AC} = -\frac{1}{\hbar c^2} \oint [\mathbf{E}(\mathbf{r}) \times \boldsymbol{\mu}] \cdot d\mathbf{r} \qquad (1)$$

where $\boldsymbol{\mu}$ is the particle magnetic dipole and $\mathbf{E}$ the electric field. Klein [16] remarked that, at first order in v/c, the AC phase can be interpreted as the interaction of the magnetic moment $\boldsymbol{\mu}$ with the motional magnetic field $\mathbf{B}_{mot} \approx -(\mathbf{v} \times \mathbf{E})/c^2$ seen by the particle in its rest frame moving with the velocity $\mathbf{v}$. In the presence of a magnetic field $\mathbf{B}$, the particle interacts with the total field $\mathbf{B}+\mathbf{B}_{mot}$ and this interaction induces a phase shift φ_{Z+AC} due to the sum of the Zeeman and AC phase effects:

$$\varphi_{Z+AC}(F, m_F) = -\frac{1}{\hbar} \oint E_{F,m_F}(|\mathbf{B} + \mathbf{B}_{mot}|)dt \qquad (2)$$

where $E_{F,m_F}(|\mathbf{B} + \mathbf{B}_{mot}|)$ is the energy of the (F, m_F) sublevel in the presence of the field. We measure the AC phase by measuring the variation of φ_{Z+AC} due to the presence of $\mathbf{B}_{mot}$. In our experiment, $B_{mot} \leq 10^{-8}$ T is always considerably smaller than $B \geq 10^{-5}$ T, and the AC phase can be written as:

$$\varphi_{AC}(F, m_F) = -\frac{1}{\hbar} \oint \frac{\partial E_{F,m_F}}{\partial B} (\mathbf{B}_{mot} \cdot \hat{\mathbf{e}}_B)\, dt \qquad (3)$$

where $\hat{\mathbf{e}}_B$ is a unit vector parallel to $\mathbf{B}$, $\hat{\mathbf{e}}_B = \mathbf{B}/B$: only the component of $\mathbf{B}_{mot}$ parallel to $\mathbf{B}$ contributes to the AC phase. For the $F = 2, m_F = \pm 2$ sublevels of ^{7}Li, no spin decoupling occurs and $\partial E_{2,\pm 2}/\partial B$ is very close to the Bohr magneton moment $\mp\mu_B$.

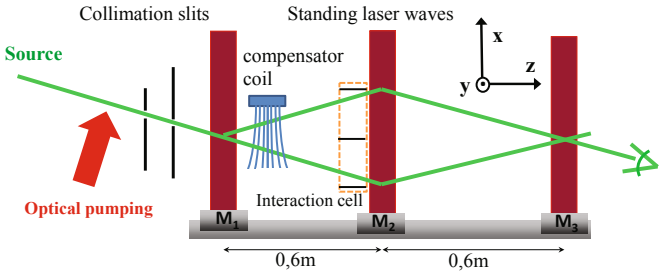

Fig. 1. Schematic top-view of our atom interferometer (not to scale): a supersonic lithium is optically pumped, collimated and crosses three laser standing waves, which diffract the atom waves in the Bragg regime. A coil, mounted at mid-distance between the first standing waves produces a compensating magnetic field gradient. The interaction cell is mounted just before the second laser standing wave (see Fig. 2 for details).

4 Our experimental setup

4.1 The atom interferometer

Our Mach-Zehnder atom interferometer has been described in detail [17] and it is schematically represented in Figure 1. The atomic beam is produced by a supersonic expansion of natural lithium seeded in a large excess of a noble gas which fixes the mean beam velocity v_m of the lithium atoms: v_m scales like $1/\sqrt{M}$, where M is the noble gas atomic mass (see Tab. 2). The beam velocity distribution is well described by a Gaussian [18,19] with a $1/e$ half-width equal to $v_m/S_\parallel$ where $S_\parallel$ is the parallel speed ratio. $S_\parallel$ depends on the source parameters (nozzle diameter, pressure, temperature, carrier gas): in our experiments, its typical value is $S_\parallel \approx 7$, which corresponds to a distribution with a FWHM of 24%.

The lithium beam is first optically pumped and collimated. Then, it crosses three laser standing waves which diffract the atom wave in the Bragg regime: first-order diffraction is used to split, reflect and recombine the atomic waves. The laser used to produce the standing waves is a single frequency dye laser. Its wavelength λ_L is chosen on the blue side of the $^2S_{1/2} \rightarrow {}^2P_{3/2}$ transition of ^{7}Li at 671 nm: this choice and the natural abundance of ^{7}Li (92.5%) explain the fact, that only ^{7}Li contributes to

Table 2. The mean lithium beam velocity v_m, the mean signal intensity I_0, the fringe visibility $\mathcal{V}$ and the phase sensitivity φ_{min} measured with the three carrier gases. I_0 is large with neon and argon but considerably smaller with krypton, while $\mathcal{V}$ has opposite variations. φ_{min} has comparable values with neon and argon and is about half as much with krypton.

Carrier gas M (a.m.u.)	v_m (m/s)	I_0 (10^3 c/s)	$\mathcal{V}$ %	φ_{min} mrad/$\sqrt{\text{Hz}}$
Ne: 20.2	1520 ± 38	56	60	7.0
Ar: 39.9	1062 ± 20	33	75	7.3
Kr: 83.8	744 ± 18	7	80	14.9

the interferometer signal [20]. This signal can be written as:

$$I = I_0 \left[1 + \mathcal{V} \cos\left(\varphi_d + \varphi_p\right)\right] \quad (4)$$

where I_0 is the mean signal intensity and $\mathcal{V}$ the fringe visibility. φ_d is the diffraction phase, $\varphi_d = 4\pi(x_1 - 2x_2 + x_3)/\lambda_L$ with x_i the position of the mirror M_i ($i = 1, 2, 3$), and φ_p the phase due to various perturbations. For one second data recording, the phase sensitivity (the minimum detectable phase) is proportional to $\varphi_{min} = 1/(\mathcal{V}\sqrt{I_0})$. Table 2 summarizes the typical values of I_0, $\mathcal{V}$ and φ_{min} as a function of the carrier gas used in our experiment.

The lithium de Broglie wavelength is $\lambda_{dB} = 5.7 \times 10^{-8}/v_m$, with λ_{dB} in m and v_m in m/s, and the first order diffraction angle is $\theta = 2\lambda_{dB}/\lambda_L \approx 0.17/v_m$ rad, for example, with argon as a carrier gas, $\lambda_{dB} \approx 54$ pm and $\theta \approx 160$ μrad. The distance between the interferometer arms, which is maximum at the second laser standing wave, is approximately equal to 143 (krypton), 100 (argon) and 70 μm (neon), which is sufficient to introduce a septum [21] between the two interferometer arms.

4.2 The interaction cell

We have built the present experiment to measure the HMW phase shift, using an arrangement inspired by the ideas of Wei et al. [22], with opposite electric fields on the two interferometer arms and a common homogeneous magnetic field [6,23]. Figure 2 shows the interaction cell. It consists of a double plane capacitor used to produce the needed electric fields and the capacitor assembly is inserted in a support which holds two coils producing the magnetic field.

The two capacitors share the septum as a common, grounded electrode. The electric field vector lies on the horizontal plane, with opposite values on the two interferometer arms and a magnitude of $E_{max} \approx 0.7$ MV/m for the maximum applied voltage $V = 800$ V and it extends over a 48 mm length. Each high voltage electrode is separated by 1 mm-wide gaps from two 5 mm-long grounded guard electrodes, in order to have well defined fringing fields.

The two coils produce a magnetic field **B** along the vertical axis. With the largest current used in the present experiments, $I = 40$ A, the field is equal to $B_{max} = 22.4$ mT. This magnetic field is needed for the observation of the HMW effect but its presence is also important for the observation of the AC phase, as discussed in equation (3) and also because the magnetic moment of a hyperfine-Zeeman sublevel is parallel or antiparallel to the local magnetic field.

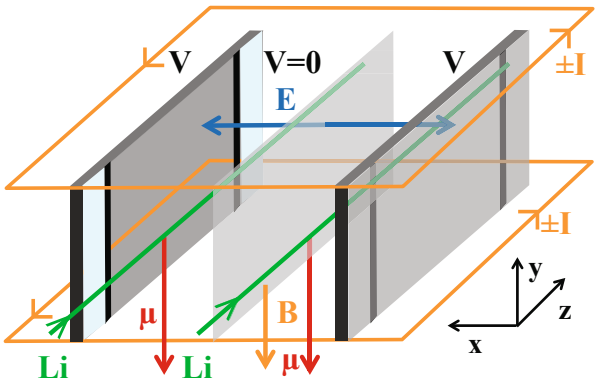

Fig. 2. Schematic drawing of our interaction cell (not to scale). A double capacitor produces opposite electric fields **E** (blue) in the horizontal plane. The high voltage electrodes are surrounded by grounded guard electrodes (light blue). Two coils (yellow) produce a vertical magnetic field **B**. The magnetic dipole (red) $\boldsymbol{\mu}$ is parallel or antiparallel to the magnetic field, depending on the pumped level. Each interferometers arm (green) passes through a different capacity.

The magnetic field produced in the interaction region has a small gradient along the x-direction so that it has slightly different values on the two interferometer arms. This difference induces a Zeeman phase shift equal to 18 rad for the largest magnetic field. As this phase shift is a function of the atom velocity v, proportional to v^{-2}, the velocity dispersion of our atom beam reduces the fringe visibility to a very low value when $B = B_{max}$: with our velocity distribution ($S_{\|} \approx 7$), the visibility and therefore the phase sensitivity are reduced by a factor of about 20. It is possible to compensate this Zeeman phase shift by applying an opposite gradient at another place in the interferometer: this is done by a compensator coil located at mid-distance between the first two laser standing waves (see Fig. 1). We are thus able to cancel the Zeeman phase shift and to keep a large value of the fringe visibility. It is not necessary to obtain an exact cancellation of the Zeeman phase shift as our acquisition protocol described below rejects the residual Zeeman phase shift.

4.3 Optical pumping of the lithium atoms

The lithium atoms are optically pumped in one Zeeman-hyperfine sublevel $F = 2, m_F = +2$ (or $m_F = -2$) of their $^2S_{1/2}$ ground state [24]. The optical pumping is performed before beam collimation in order to avoid heating the transverse motion by exchange of photon momenta. We control the magnetic field in the pumping region by three pairs of square Helmholtz coils. The D1 line of lithium is used because its hyperfine components are better resolved than those of the D2 line, due to the larger hyperfine splitting of the $^2P_{1/2}$ state and this is a favorable condition for

Table 3. The measured population $P(F=2,m_F)$ after optical pumping for different atom velocities v_m [24].

v_m (m/s)	m_F	$P(F=2,m_F)$
744	+2	(96 ±6) %
	−2	(93 ±7) %
1062	+2	(100 ±13)%
	−2	(95 ±11)%
1520	+2	(90 ±1) %
	−2	(94 ±2) %

a very efficient optical pumping. Two circularly polarized laser beams are tuned to the $^2S_{1/2}, F=1 \rightarrow {}^2P_{1/2}, F=2$ and the $^2S_{1/2}, F=2 \rightarrow {}^2P_{1/2}, F=2$ transitions. The first laser beam empties the $F=1$ level, while the second one pumps the atoms into the $F=2, m_F=\pm 2$ level, depending on the chosen circular polarization and on the magnetic field direction.

As discussed below, we separate the HMW and AC phases by reversing the m_F value which is obtained by reversing the magnetic field in the pumping region. The m_F value measured on an axis parallel to the local magnetic field is conserved along the atom propagation, if the condition for an adiabatic transport is fulfilled. This condition is verified experimentally with our measurements of the pumping efficiency. This pumping efficiency has been characterized by an atom interferometric method and we have found that the pumped sublevel has a fraction of the total population near 95 ± 5% [24]. Our results are recalled in Table 3.

5 Measurements of the AC phase shift

5.1 The topological nature of the AC phase

As pointed out by Cimmino and Klein [25] the experiments with atoms and molecules quoted in Table 1 do not test the topological nature of the AC phase. In a recent publication, McKellar et al. [26] discussed the three criteria which must be fulfilled to test the topological nature of the AC phase:

1. $\boldsymbol{\nabla} \times (\boldsymbol{\mu} \times \mathbf{E}) = 0$ must be verified on the interferometer arms.
2. There must be an excluded region between these arms where $\boldsymbol{\nabla} \times (\boldsymbol{\mu} \times \mathbf{E}) \neq 0$.
3. The phase shift should be velocity independent.

The two last criteria are fulfilled by all experiments with atoms or molecules quoted in Table 1, but only the neutron experiment of Cimmino et al. [10] satisfies the first criterion. In our set-up the magnetic moment orientation is the same on both interferometer arms. The electric field is orthogonal to the magnetic moment, it is parallel to the interferometer plane and $\boldsymbol{\nabla} \times (\boldsymbol{\mu} \times \mathbf{E})$ is zero in the arm region. A small difference from zero may arise from experimental imperfections of the capacitors and magnetic field geometries. The second criterion is also satisfied and the third one is verified by our experimental results as shown in Section 6.2. Consequently, our experiment fulfills all three criteria given above and can prove the topological nature of the AC phase.

5.2 Measurement protocol

As explained in our previous papers [6,7,23], we eliminate interferometer phase drifts by alternating several configurations of the electric and magnetic fields in the interaction cell. These configurations are characterized by the voltage V applied to the capacitor and by the current I circulating in the coil and we use 6 different configurations (V,I), $(V,0)$, $(0,I)$, $(-V,0)$, $(-V,I)$ and $(0,0)$, each one being applied 8 times during each 20 seconds-long fringe scan. Least-square fits are used to extract the phase $\varphi(V,I,m_F)$ corresponding to each field configuration and to an optical pumping in the $F=2, m_F=+2$ sublevel. We reduce the statistical uncertainty by averaging the results of about 80 similar fringe scans. Successive experiments are made with opposite values of the current I and the m_F value.

5.3 Extraction of the AC phase shift

Five effects contribute to the measured phase shifts. Two of them are the residual phases due to the Stark effect and to the Zeeman effect: these phases are produced by the differences of electric fields and magnetic fields on the two interferometer arms. The third contribution is the HMW phase $\varphi_{HMW}(V,I)$ and the last two contributions are the AC phases $\varphi_{AC}(V,I)$ and $\varphi_{AC}(V,I=0)$, the latter is due to the residual laboratory magnetic field. It is easy to verify that the residual Stark and Zeeman phases are eliminated by the following combination of measured phases:

$$\varphi_{EB}(V,I,m_F) = \varphi(V,I) - \varphi(V,0) - \varphi(0,I) + \varphi(0,0). \quad (5)$$

$\varphi_{EB}(V,I,m_F)$ is solely due the HMW and AC phases and it is equal to:

$$\varphi_{EB}(V,I,m_F) = \varphi_{HMW}(V,I) + \varphi_{AC}(V,I,m_F) - \varphi_{AC}(V,I=0,m_F). \quad (6)$$

Following equation (3), $\varphi_{AC}(V,I=0,m_F)$ is sensitive to the laboratory residual magnetic field $\mathbf{B}_{lab}$ when $I=0$. B_{lab} is about 35 μT and the field is mainly oriented downwards along the y-axis. If we apply a coil current $I \geq 5$ A, the coil magnetic field B_{coil} is always larger than 2.8 mT and $\mathbf{B} = \mathbf{B}_{coil} + \mathbf{B}_{lab}$ is nearly perfectly vertical. As the HMW phase does not depend on m_F while the AC phase changes sign with m_F, we extract the contributions due to the AC phase thanks to the linear combination:

$$\varphi_{AC}^{exp}(V,I) = \left[\varphi_{EB}(V,I,2) - \varphi_{EB}(V,I,-2)\right]/2. \quad (7)$$

Following equation (6), $\varphi_{AC}^{exp}(V,I)$ should be equal to the theoretical value:

$$\varphi_{AC}^{exp}(V,I) = \varphi_{AC}(V,I,2) - \varphi_{AC}(V,I=0,2). \quad (8)$$

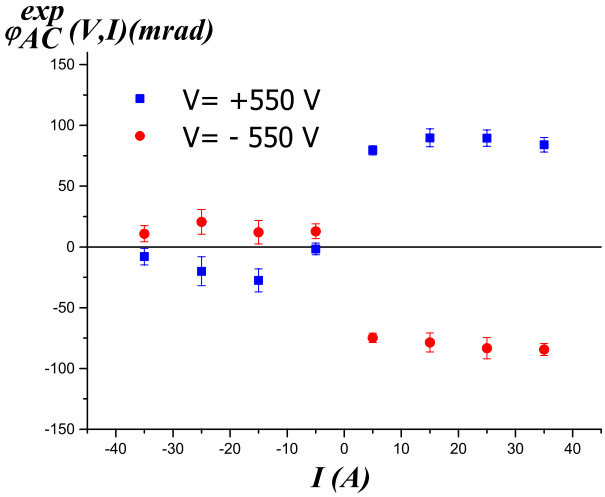

Fig. 3. The AC phase $\varphi_{AC}^{exp}(V,I)$ defined by equation (7) is plotted as a function of the applied current for two voltages $V = \pm 550$ V. The sign $\varphi_{AC}(V,I,m_F)$ is related to the sign of I and its absolute value is larger than $\varphi_{AC}(V,I=0,m_F)$, due to the better verticality of $\mathbf{B}$, as shown by equation (3).

5.4 Effects of the laboratory residual magnetic field

Figure 3 shows typical measurements of the AC phase $\varphi_{AC}^{exp}(V,I)$ for two voltages $V = \pm 550$ V as a function of the current I. For a given sense of I, $\varphi_{AC}^{exp}(V,I)$ does not vary significantly with the current as expected but $\varphi_{AC}^{exp}(V,I)$ changes sign when we reverse the current I and the magnetic field $\mathbf{B}$. For $I \leq -5$ A, $\mathbf{B}$ is pointing in a direction opposite to the one of $\mathbf{B}_{lab}$ and $\varphi_{AC}(V,I,m_F)$ has a sign opposite to the one of $\varphi_{AC}(V,I=0,m_F)$. As the modulus of $\varphi_{AC}(V,I,m_F)$ is larger than the one of $\varphi_{AC}(V,I=0,m_F)$, the modulus of $\varphi_{AC}^{exp}(V,I)$ is small but non vanishing when $I \leq -5$ A. For $I \geq 5$ A, the situation is reversed, with $\varphi_{AC}(V,I,m_F)$ and $\varphi_{AC}(V,I=0,m_F)$ having the same sign and adding their contributions to $\varphi_{AC}^{exp}(V,I)$.

5.5 The measured AC phase shift

Using equation (8), the AC phase in the presence of the applied magnetic field $\mathbf{B}$, $\varphi_{AC}(V,I,2)$, can be extracted by the linear combination, i.e. the common phase $\varphi_{AC}(V,I=0,2)$ is rejected:

$$\varphi_{AC}(V,|I|) = \frac{1}{2}\left[\varphi_{AC}^{exp}(V,I) - \varphi_{AC}^{exp}(V,-I)\right] \qquad (9)$$

and $\varphi_{AC}(V,|I|)$ must be equal to the theoretical value of the AC phase for the sublevel $m_F = +2$. Figure 4 presents our measurements $\varphi_{AC}(V,|I|)$ as a function of V for an experiment with a mean lithium velocity $v_m = 1062$ m/s. We have performed similar experiments and data analysis with the two other mean velocities of the lithium beam. The results are collected in Table 4 and plotted in Figure 5.

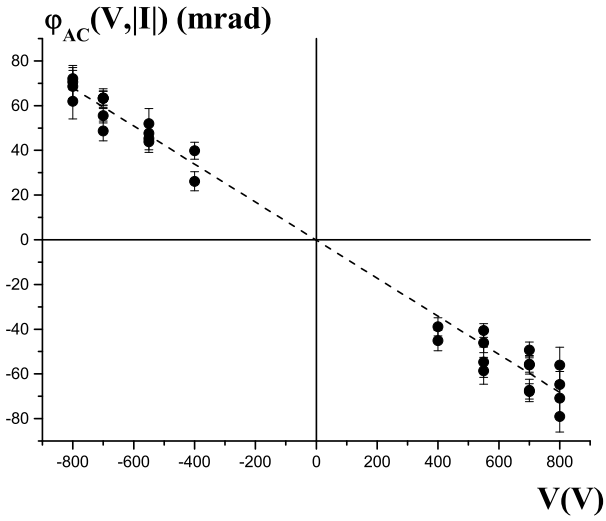

Fig. 4. The AC phase $\varphi_{AC}(V,|I|)$, defined by equation (9), is plotted as a function of the applied voltage V for an experiment with a mean lithium velocity $v_m = 1062$ m/s. Each data point (black circle) is plotted with its 1σ error bar and, for a given voltage V, there are several points corresponding to different values of the current $|I|$. These measurements are in good agreement with a linear behavior, as shown by the dashed line which represents the best least-square fit. The fitted slope is equal to $(-8.51 \pm 0.18) \times 10^{-5}$ rad/V while the fitted offset, equal to 0.2 ± 1.2 mrad, is compatible with 0, which is expected as the AC phase vanishes with the electric field.

Table 4. Our measurements of the AC phase slope $\partial\varphi_{AC}/\partial V$ in 10^{-5} rad/V are compared to the theoretical values $\partial\varphi_{AC}^{c}/\partial V$ corrected for imperfect optical pumping (see Eq. (10)). These predicted values show a velocity dependence, which stems from the velocity dependence of the optical pumping efficiency.

v_m (m/s)	$\partial\varphi_{AC}/\partial V$ experiment	$\partial\varphi_{AC}^{c}/\partial V$ theory
1520 ± 18	-8.05 ± 0.20	-7.86 ± 0.12
1062 ± 20	-8.51 ± 0.18	-8.51 ± 0.88
744 ± 18	-8.44 ± 0.41	-8.40 ± 0.48

6 Comparison of the measured AC phase shift with theory

6.1 The theoretical value of the AC phase for the $F = 2, m_F = \pm 2$ sublevels

The theoretical value of the AC phase slope versus applied voltage is deduced from equation (3). When the applied magnetic field is sufficiently large (in practice when the current in the coils of the interaction cell verifies $|I| \geq 5$ A), the vector $\mathbf{e}_B$ which measures the direction of the total magnetic field is vertical and the motional magnetic field $\mathbf{B}_{mot}$ is parallel to $\mathbf{e}_B$. We must calculate the integral of the electric field over the length of the capacitor and our procedure was described in a previous paper [23]. We may recall briefly how we proceed: the capacitor lengths were measured and found equal to

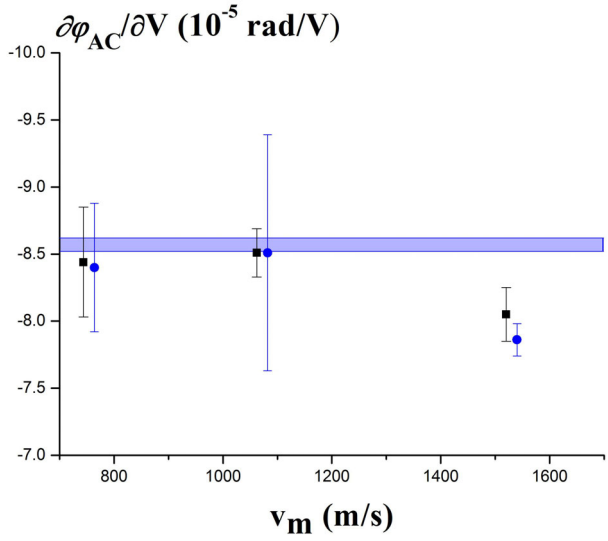

Fig. 5. Plot of the slope of the AC phase $\partial\varphi_{AC}(V)/\partial V$ as a function of the mean atom velocity v_m. The experimental results (black squares) are compared to the theoretical value calculated with the assumption of a perfect optical pumping (blue horizontal band) and to the theoretical values $\partial\varphi^c_{AC}/\partial V$ corrected for imperfect optical pumping (blue circles slightly displaced at the right of the experimental values for better visibility).

(48 ± 0.5) mm and we deduce the spacing value of each capacitor from the measurements of the Stark phase shifts produced by this capacitor and from the theoretical value of the polarizability of lithium which calculated with a very high accuracy [27,28]. For $F = 2, m_F = \pm 2$ sublevel, no spin decoupling occurs and $\partial E_{2,\pm 2}/\partial B = -g_F m_F \mu_B$, where g_F is the Landé factor. Taking into account the nuclear spin $I = 3/2$, $g_F = (g_J + 3g_I)/4$, where g_J is the Landé factor of the $^2S_{1/2}$ ground state and g_I is the Landé factor of the nuclear spin. Both factors are known with a high precision [29,30] and from these values we calculate $g_F = -0.4996886$. We thus predict an AC phase slope $|\partial\varphi_{AC}/\partial V| = (8.57 \pm 0.05) \times 10^{-5}$ rad/V where the uncertainty of the AC phase is dominated by the uncertainty on the capacitor geometry.

6.2 The effect of imperfect optical pumping

However, the optical pumping is not perfect and we must take this defect into account for a more realistic estimate of the AC phase. The interferometer signal (Eq. (4)) is the sum of the contributions of the 8 Zeeman-hyperfine sublevels:

$$I = I_0 \sum_{F,m_F} P(F,m_F) \times [1 + \mathcal{V}(F,m_F)\cos(\varphi_d + \varphi_{AC}(F,m_F))] \quad (10)$$

where $P(F,m_F)$ is the normalized population of the F,m_F sublevel and, for simplicity, we have omitted all the perturbation phases except the AC phase. The contributions of the $m_F \neq \pm 2$ sublevels play a minor role for three reasons: their populations are small, the AC phase change sign with the sublevel and the visibility $\mathcal{V}(F,m_F)$ of their contributions should be small, because the compensator produces a low magnetic field which compensates exactly the Zeeman phase shift only for the $m_F = \pm 2$ sublevels for which the Zeeman effect is purely linear. As a consequence, we consider that the contributions from the $m_F \neq \pm 2$ sublevels can be neglected and then, a straightforward calculation shows that our experiment measures a corrected AC phase given by:

$$\varphi^c_{AC}(m_F) = \varphi_{AC}(m_F)\frac{P(2,m_F) - P(2,-m_F)}{P(2,m_F) + P(2,-m_F)} \quad (11)$$

when the optical pumping aims at populating the $F = 2$, m_F sublevel. We thus get more realistic theoretical estimates of the measured AC phases (see Tab. 4) with errors bars which take into account the errors on the population measurements [24] and on the capacitor geometry. We want to point out that the velocity dependence of $\varphi^c_{AC}(m_F)$ is solely due to the fact that the measured efficiency of the optical pumping is a function of the atom velocity. Our measurements are in excellent agreement with these corrected theoretical values, as illustrated in Figure 5. Our measurements give a further proof of the independence of the AC phase with the atom velocity and an important limitation of this test comes from the limited accuracy with which we have measured the optical pumping efficiency.

7 Conclusion

In conclusion, we have measured the Aharanov-Casher (AC) phase by atom interferometry using optically pumped lithium atoms. Our separated arm interferometer operates with atoms in a single internal quantum state and two opposite electric fields are applied on the interferometer arms to realize the AC measurements. This approach to measure the AC phase is new, as all previous works used either unpolarized neutrons [10] or Ramsey or Ramsey-Bordé interferometers with atoms and molecules [11–15]. Moreover, our experiment is the first one to fully test the topological nature of the AC phase with atoms.

Our measurements were performed during the study of the He-McKellar-Wilkens (HMW) phase and we had not optimized the setup for the measurement of the AC phase. In particular, a better control of the residual magnetic field in the interaction region would have simplified the analysis. We have verified that the AC phase depends linearly on the electric field strength. We have performed AC phase measurements for three different mean velocities of the atomic beam (744, 1062 and 1520 m/s) and these measurements are in good agreement with the fact that this phase does not depend on the atom velocity, a characteristic of a geometric phase. Our measurements, with a statistical uncertainty close to 3%, agree with their theoretical estimates, which have a considerably larger uncertainty due to their sensitivity to the population distribution over the Zeeman-hyperfine sublevels. The optical

pumping of the lithium beam is quite efficient, with about $95 \pm 5\%$ of the population transferred in the pumped sublevel, but a better pumping, which is feasible [31], would reduce the uncertainty on the theoretical values of the AC phase.

We thank the laboratory technical and administrative staff for their help. We thank H. Batelaan and A. Cronin for fruitful discussions, G. Trénec, A. Miffre and M. Jacquey for all the work done on our atom interferometer. We thank CNRS INP, ANR (Grants ANR-05-BLAN-0094 and ANR-11-BS04-016-01 HIPATI) and Région Midi-Pyrénées for support.

References

1. Y. Aharonov, A. Casher, Phys. Rev. Lett. **53**, 319 (1984)
2. J. Anandan, Phys. Rev. Lett. **48**, 1660 (1982)
3. Y. Aharonov, A. Bohm, Phys. Rev. **115**, 485 (1959)
4. X.-G. He, B.H.J. McKellar, Phys. Rev. A **47**, 3424 (1993)
5. M. Wilkens, Phys. Rev. Lett. **72**, 5 (1994)
6. S. Lepoutre, A. Gauguet, G. Trénec, M. Büchner, J. Vigué, Phys. Rev. Lett. **109**, 120404 (2012)
7. J. Gillot, S. Lepoutre, A. Gauguet, M. Büchner, J. Vigué, Phys. Rev. Lett. **111**, 030401 (2013)
8. M.V. Berry, Proc. R. Soc. Lond. A **392**, 45 (1984)
9. A. Shapere, F. Wilczek, *Geometric Phases in Physics* (World Scientific, Singapore, 1989)
10. A. Cimmino, G.I. Opat, A.G. Klein, H. Kaiser, S.A. Werner, M. Arif, R. Clothier, Phys. Rev. Lett. **63**, 380 (1989)
11. K. Sangster, E.A. Hinds, S.M. Barnett, E. Riis, Phys. Rev. Lett. **71**, 3641 (1993)
12. K. Sangster, E.A. Hinds, S.M. Barnett, A.G. Sinclair, Phys. Rev. A **51**, 1776 (1995)
13. A. Görlitz, B. Schuh, A. Weis, Phys. Rev. A **51**, R4305 (1995)
14. K. Zeiske, G. Zinner, F. Riehle, J. Helmcke, Appl. Phys. B **60**, 205 (1995)
15. S. Yanagimachi, M. Kajiro, M. Machiya, A. Morinaga, Phys. Rev. A **65**, 042104 (2002)
16. A.G. Klein, Physica **65**, 230 (1986)
17. A. Miffre, M. Jacquey, M. Büchner, G. Trénec, J. Vigué, Eur. Phys. J. D **33**, 99 (2005)
18. J.P. Toennies, K. Winkelmann, J. Chem. Phys. **1977**, 3965 (1977)
19. D.R. Miller, in *Atomic and Molecular Beam Methods*, edited by G. Scoles, D. Bassi, U. Buck, D.C. Laine (Oxford University Press, 1998), pp. 14–53
20. M. Jacquey, A. Miffre, M. Büchner, G. Trénec, J. Vigué, Europhys. Lett. **77**, 20007 (2007)
21. C.R. Ekstrom, J. Schmiedmayer, M.S. Chapman, T.D. Hammond, D.E. Pritchard, **51**, 3883 (1995)
22. H. Wei, R. Han, X. Wei, Phys. Rev. Lett. **75**, 2071 (1995)
23. S. Lepoutre, J. Gillot, A. Gauguet, M. Büchner, J. Vigué, Phys. Rev. A **88**, 043628 (2013)
24. J. Gillot, A. Gauguet, M. Büchner, J. Vigué, Eur. Phys. J. D **67**, 263 (2013)
25. A. Cimmino, A.G. Klein, Physica B **385-386**, 1392 (2006)
26. B.H.J. McKellar, X.-G. He, A.G. Klein, AIP Conf. Proc. **1588**, 59 (2014)
27. M. Puchalski, D. Kedziera, K. Pachucki, Phys. Rev. A **84**, 052518 (2011)
28. M. Puchalski, D. Kedziera, K. Pachucki, Phys. Rev. A **85**, 019910 (2012)
29. E. Arimondo, M. Inguscio, P. Violino, Rev. Mod. Phys. **49**, 31 (1977)
30. Z.-C. Yan, Phys. Rev. Lett. **86**, 5683 (2001)
31. G.W. Schinn, X.L. Han, A. Gallagher, J. Opt. Soc. Am. B **8**, 169 (1991)